Foundations of Materials Simulation
Atomistic Simulation

Atharva Sinnarkar

18 January 2025

Abstract

This report presents a comprehensive study of atomistic simulations applied to the structural and mechanical properties of FCC copper. The investigation begins with an analysis of interatomic potentials, comparing pair-potential models with the Effective-Medium Theory (EMT) and assessing their applicability in metal simulations.

The equilibrium lattice parameters and cohesive energy of copper are computed, followed by the determination of elastic constants (C_{11}, C_{12}, C_{44}) using energy-strain relationships. A polynomial fitting approach is employed to extract mechanical properties from molecular dynamics simulations. Additionally, the validity of the quadratic energy-strain assumption is examined, revealing deviations at higher strain values.

The results demonstrate the effectiveness of atomistic modeling in capturing essential material properties while highlighting limitations in potential models at large deformations.

Contents

List of Figures

List of Tables

1 Introduction

Atomistic simulations play a crucial role in understanding material behavior at the atomic scale, offering valuable insights into structural stability, defect mechanics, and mechanical properties. These simulations rely on interatomic potential models to approximate interactions between atoms, influencing the accuracy of computed material properties.

This report focuses on the effectiveness of different interatomic potentials in modeling metallic systems, particularly copper. A comparative study is conducted between pair-potential models and the Effective-Medium Theory (EMT) to assess their suitability for metal simulations.

Furthermore, computational methods are employed to determine key material properties, including the equilibrium lattice constant, cohesive energy, and elastic stiffness constants C_{11}, C_{12}, C_{44}. The energy-strain relationship is analyzed using LAMMPS-based molecular dynamics simulations combined with Python-based polynomial fitting techniques to extract mechanical properties.

Additionally, the study examines the validity of the quadratic approximation in the energy-strain relationship, identifying deviations at higher strain values and highlighting the need for higher-order corrections in large deformation scenarios.

Through this analysis, the report demonstrates the effectiveness of atomistic modeling in predicting material behavior while also addressing the limitations of potential models in capturing complex interactions in metallic systems.

2 Methodology

2.1 Comparison of Interaction Potentials

The interaction energy for pair-potential and EMT models is compared in Table 1.

Parameter	Pair-Potential Model	Effective-Medium Theory
Mathematical Form	The interaction energy is calculated using the Lennard-Jones formula: $$V_{int} = \frac{1}{2}\sum_{\alpha,\beta}\phi_{\alpha\beta}(r_{\alpha\beta})$$ where: $$\phi(r) = 4\epsilon\left[\left(\frac{\sigma}{r}\right)^{12} - \left(\frac{\sigma}{r}\right)^{6}\right]$$ **Key parameters:** • σ: distance parameter • ϵ: energy parameter • r: interatomic separation	The total energy incorporates pair interactions and many-body effects: $$V_{int} = \frac{1}{2}\sum_{\alpha,\beta}\phi_{\alpha\beta}(r_{\alpha\beta}) + \sum_{\alpha}U_{\alpha}(\rho_{\alpha})$$ where: • $\phi_{\alpha\beta}$: pair interaction term • U_{α}: embedding energy function • ρ_{α}: electron density contribution
Atomic Environmental Effects	Only considers pairwise interactions, ignoring surrounding atomic environment and density effects.	Includes local electronic density effects via the embedding function U_{α}, capturing the collective influence of neighboring atoms.
Computational Efficiency	Scales as $\mathcal{O}(N)$, where N is the total atom count.	Computational cost is higher due to additional embedding function calculations, approximately doubling the cost of pair potentials.
Application Domains	Best suited for: • Ionic systems with dominant Coulomb interactions • Simple molecular systems	Effectively models: • Simple metals • Transition metals (filled/near-filled d-orbitals) • Basic metallic alloys • Dilute solid solutions

Table 1: Comparative Analysis of Interaction Potential Models

2.2 Limitations of Pair Potentials in Metallic Systems

While pair potentials are widely used in computational material simulations, they exhibit inherent shortcomings when applied to metallic systems. The key limitations are as follows:

1. **Lack of Many-Body Effects:** Traditional pair potential models assume that the total interaction energy is a sum of individual atomic interactions, ignoring collective electronic influences. However, in metallic systems, bonding arises from delocalized electrons, requiring many-body interactions to accurately capture material properties.

2. **Incorrect Energy Scaling:** The binding energy in metals does not scale linearly with the number of neighboring atoms. Pair potentials fail to account for electron density redistribution when introducing defects such as vacancies or interstitials, leading to inaccurate predictions of defect formation energies.

Despite these drawbacks, pair potentials offer certain computational advantages:

- **Lower Computational Cost:** Since pairwise interactions involve fewer calculations, they enable efficient large-scale simulations compared to many-body potentials.

- **Fundamental Role in Hybrid Models:** Pair potentials serve as a foundational element in more advanced models, including:

  - Modeling van der Waals interactions effectively.
  - Providing an initial approximation for tight-binding calculations.
  - Enhancing hybrid potential models like Embedded Atom Method (EAM) and Finnis-Sinclair potentials.

2.3 Parameter Identification and Fitting Strategies

To accurately model interatomic interactions, potential parameters must be fitted using robust methods. The comparison of parameter identification between pair potentials and Effective-Medium Theory (EMT) is summarized in Table 2.

Aspect	Pair Potential	EMT/Semi-Empirical
Number of Parameters	Minimal: distance parameter (σ) and energy scale (ϵ), typically derived from experimental data or simple force fitting.	Complex: requires multiple parameters including electron density functions, embedding energies, and pair interaction terms.
Fitting Method	Direct parameter optimization based on bulk material properties such as equilibrium bond length, cohesive energy, and elastic moduli.	Multi-step fitting approach involving: • Density Functional Theory (DFT) force matching • Parameter tuning for embedding functions • Validation against experimental elastic properties.

Table 2: Comparison of Parameter Identification Methods

2.4 Copper Potential Parameters

A detailed literature review has provided key crystallographic properties essential for simulating copper. These parameters are widely used in atomistic modeling to ensure accuracy in structural and energetic calculations.

Property	Value	Units
Crystal Structure	Face-Centered Cubic (FCC)	-
Lattice Constant (300K)	3.615	Å
Nearest Neighbor Distance	2.556	Å
Atomic Volume	11.82	$Å^3$
Cohesive Energy	3.54	eV/atom

Table 3: Crystallographic properties of copper

The FCC structure of copper, characterized by a lattice parameter of 3.615 Å at room temperature, aligns well with experimental and computational findings. Additionally, the cohesive energy of 3.54 eV/atom has been confirmed through first-principles calculations and experimental data.

These parameters can be directly implemented in computational frameworks such as the LAMMPS using the Effective-Medium Theory (EMT) potential. Since the EMT potential is pre-parameterized for copper, it simplifies integration into molecular dynamics simulations without requiring additional parameter fitting.

The crystallographic features and general physical properties of copper used in the simulation are listed in Tables 1.1 and 1.2 of (1).

3 Geometric Analysis of Cubic Structures

Understanding the geometric relationships in crystal structures is essential for evaluating atomic arrangements and interatomic distances. This section provides an analytical derivation of lattice parameters for Face-Centered Cubic (FCC) and Body-Centered Cubic (BCC) structures.

3.1 Face-Centered Cubic (FCC) Lattice

For an FCC structure, the atomic arrangement follows a cubic symmetry where atoms are positioned at the corners and the centers of each face. The lattice parameter is derived using elementary trigonometry:

$$\sqrt{l^2 + l^2} = 4a \tag{1}$$

$$l = 2a\sqrt{2} \tag{2}$$

where l represents the lattice parameter and a denotes the atomic radius.

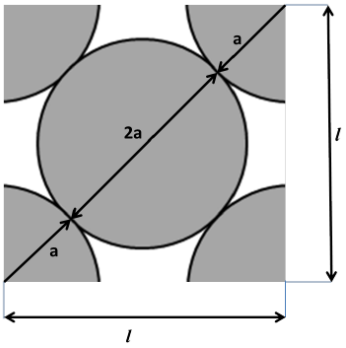

Figure 1: Schematic of Face-Centered Cubic (FCC) structure

3.2 Body-Centered Cubic (BCC) Lattice

In the BCC structure, the atomic arrangement consists of atoms at the corners of the unit cell and one additional atom at its center. The lattice parameter is determined by considering the body diagonal of the cube:

$$(4a)^2 = (\sqrt{2}l)^2 + l^2 \tag{3}$$

$$l = \frac{4a}{\sqrt{3}} \tag{4}$$

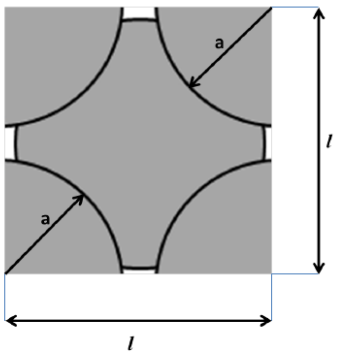

Figure 2: Schematic of Body-Centered Cubic (BCC) structure

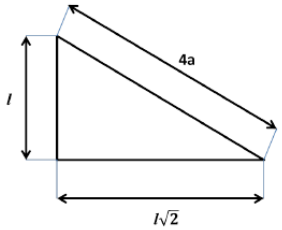

Figure 3: Close-packed plane in BCC structure

4 Lattice Energy Minimization

To determine the equilibrium lattice constant of a material, we employ quadratic fitting of the potential energy as a function of lattice parameter l. The total energy W is approximated using a second-order polynomial:

$$W = p_0 + p_1 l + p_2 l^2 \tag{5}$$

where p_0, p_1, and p_2 represent the quadratic fitting coefficients. The equilibrium lattice constant l_0, corresponding to the **minimum energy configuration**, is obtained by differentiating W with respect to l and solving for the critical point:

$$l_0 = \frac{-p_1}{2p_2} \tag{6}$$

The corresponding minimum potential energy is then determined by evaluating $W(l_0)$:

$$W_0 = W(l_0) \tag{7}$$

4.1 Results and Discussion

Using molecular dynamics simulations in LAMMPS and quadratic curve fitting in Python, we extracted optimal lattice parameters and associated energy values for FCC, BCC, and SC structures.

4.1.1 Face-Centered Cubic (FCC)

The dataset used for FCC lattice constant optimization includes:

- Lattice constants (Å):

$$\begin{bmatrix} 3.40 & 3.41 & 3.42 & 3.43 & 3.44 & 3.45 & 3.46 & 3.47 \\ 3.48 & 3.49 & 3.50 & 3.51 & 3.52 & 3.53 & 3.54 & 3.55 \\ 3.56 & 3.57 & 3.58 & 3.59 & 3.60 & 3.61 & 3.62 & 3.63 \\ 3.64 & 3.65 & 3.66 & 3.67 & 3.68 & 3.69 & 3.70 & 3.71 \end{bmatrix}$$

- Corresponding potential energies (eV):

$$\begin{bmatrix} -1670.80 & -1680.65 & -1689.91 & -1698.59 & -1706.69 & -1714.24 & -1721.26 & -1727.74 \\ -1733.71 & -1739.17 & -1744.14 & -1748.65 & -1752.68 & -1756.26 & -1759.40 & -1762.11 \\ -1764.41 & -1766.29 & -1767.78 & -1768.88 & -1769.60 & -1769.96 & -1769.96 & -1769.61 \\ -1768.93 & -1767.91 & -1766.58 & -1764.94 & -1763.00 & -1760.76 & -1758.25 & -1755.45 \end{bmatrix}$$

The quadratic fit parameters are:

$$p_0 = 24199.04, \quad p_1 = -13385.08, \quad p_2 = 1850.89 \tag{8}$$

From this, the equilibrium lattice constant is:

$$l_0 = \frac{-(-13385.08)}{2 \times 1850.89} = 3.62 \text{ Å} \tag{9}$$

The minimum energy corresponding to l_0 is:

$$W_0 = -0.18 \text{ eV} \tag{10}$$

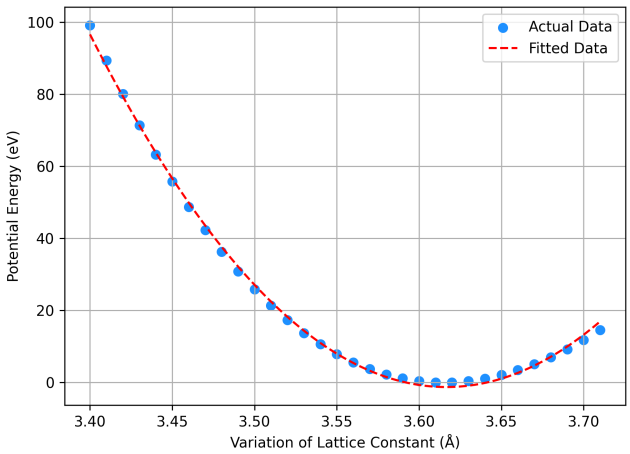

Figure 4: Quadratic fit of potential energy for FCC structure

4.1.2 Body-Centered Cubic (BCC)

The dataset for BCC lattice constant optimization is:

- Lattice constants (Å):

$$\begin{bmatrix} 2.80 & 2.81 & 2.82 & 2.83 & 2.84 & 2.85 & 2.86 & 2.87 \\ 2.88 & 2.89 & 2.90 & 2.91 & 2.92 & 2.93 & 2.94 & 2.95 \\ 2.96 & 2.97 & 2.98 & 2.99 & 3.00 & 3.01 & 3.02 & 3.03 \\ 3.04 & 3.05 & 3.06 & 3.07 & 3.08 & 3.09 & 3.10 & 3.11 \\ 3.12 & 3.13 & 3.14 & 3.15 & 3.16 & 3.17 & 3.18 & 3.19 \\ 3.20 & 3.21 & & & & & & \end{bmatrix}$$

- Corresponding potential energies (eV):

$$\begin{bmatrix} -871.12 & -873.03 & -874.60 & -875.85 & -876.78 & -877.41 & -877.77 & -877.91 \\ -877.78 & -877.38 & -876.71 & -875.80 & -874.65 & -873.27 & -871.66 & -869.83 \\ -867.79 & -865.56 & -863.13 & -860.67 & -858.17 & -855.49 & -852.64 & -849.62 \\ -846.44 & -843.11 & -839.64 & -836.02 & -832.27 & -828.39 & -824.39 & -820.27 \\ -816.03 & -811.69 & -807.25 & -802.71 & -798.08 & -793.36 & -788.55 & -783.67 \\ -778.71 & -773.64 & & & & & & \end{bmatrix}$$

The fitted quadratic coefficients are:

$$p_0 = 12259.28, \quad p_1 = -8511.26, \quad p_2 = 1476.87 \tag{11}$$

Solving for l_0:

$$l_0 = \frac{-(-8511.26)}{2 \times 1476.87} = 2.88 \text{ Å} \tag{12}$$

The corresponding minimum potential energy:

$$W_0 = 0.47 \text{ eV} \tag{13}$$

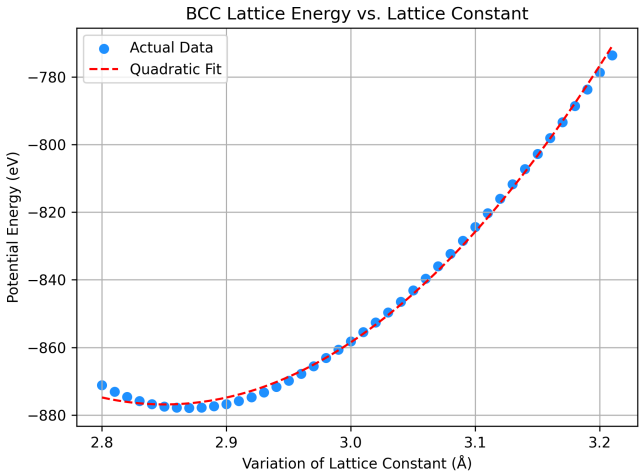

Figure 5: Quadratic fit of potential energy for BCC structure

4.1.3 Simple Cubic (SC)

For the SC structure, the dataset used for fitting includes:

- Lattice constants (Å):

$$\begin{bmatrix} 2.36000 & 2.36250 & 2.36500 & 2.36750 & 2.37000 & 2.37250 \\ 2.37500 & 2.37750 & 2.38000 & 2.38250 & 2.38500 & 2.38750 \\ 2.39000 & 2.39250 & 2.39500 & 2.39750 & 2.40000 & 2.40250 \\ 2.40500 & 2.40750 & 2.41000 & 2.41250 & 2.41500 & \end{bmatrix}$$

- Corresponding potential energies (eV):

$$\begin{bmatrix} -387.61337 & -387.72624 & -387.82713 & -387.91615 & -387.99344 & -388.05912 \\ -388.11331 & -388.15614 & -388.18773 & -388.20819 & -388.21766 & -388.21625 \\ -388.20407 & -388.18125 & -388.14789 & -388.10412 & -388.05006 & -387.98580 \\ -387.91147 & -387.82717 & -387.73302 & -387.62913 & -387.51561 & \end{bmatrix}$$

The computed quadratic fitting parameters are:

$$p_0 = 2710.77, \quad p_1 = -2305.56, \quad p_2 = 490.00 \tag{14}$$

From this, the equilibrium lattice constant is:

$$l_0 = \frac{-(-2305.56)}{2 \times 490.00} = 2.35 \text{ Å} \tag{15}$$

The corresponding minimum potential energy:

$$W_0 = 3.6 \text{ eV} \tag{16}$$

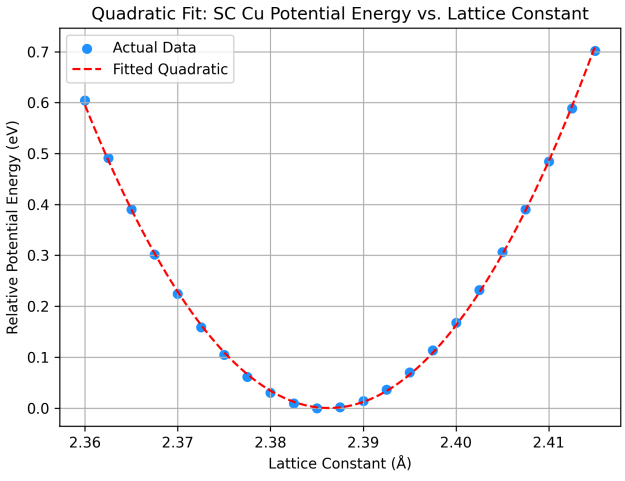

Figure 6: Quadratic fit of potential energy for SC structure

4.2 Comparison and Conclusion

The calculated equilibrium lattice constants and corresponding potential energies for each structure are summarized in Table 4.

Structure	**Lattice Formula**	p_0	p_1	p_2	l_0 (Å)	W_0 (eV)
FCC	$l = 2\sqrt{2}a$	24199.04	-13385.08	1850.89	3.62	-0.18
BCC	$l = 4a/\sqrt{3}$	12259.28	-8511.26	1476.87	2.88	0.47
SC	$l = 2a$	2710.77	-2305.56	490.00	2.385	3.6

Table 4: Computed equilibrium lattice constants and minimum energy values for FCC, BCC, and SC structures.

The obtained results confirm that the FCC structure has the lowest energy among the three, making it the most stable configuration for copper. The computed equilibrium lattice parameter for FCC ($l_0 = 3.62$ Å) is in close agreement with the literature value of 3.61 Å, showing a deviation of only 0.27%.

5 Elastic Energy Expressions in Voigt Notation

The elastic strain energy in crystalline solids can be expressed in terms of the elastic stiffness tensor and strain components. This section presents the energy formulations for specific strain states in materials with cubic symmetry, with their corresponding forms in Voigt notation.

5.1 Uniaxial Strain and Elastic Constant C_{11}

$$W^e = \frac{1}{2}\boldsymbol{\varepsilon} : \mathbf{C} : \boldsymbol{\varepsilon} \tag{17}$$

The corresponding strain tensor is:

$$\varepsilon_{ij} = \begin{bmatrix} \bar{\varepsilon} & 0 & 0 \\ 0 & 0 & 0 \\ 0 & 0 & 0 \end{bmatrix} \quad \Rightarrow \quad \varepsilon_v = \begin{bmatrix} \bar{\varepsilon} \\ 0 \\ 0 \\ 0 \\ 0 \\ 0 \end{bmatrix} \tag{18}$$

The elastic constant is then given by:

$$C_{11} = \frac{2W^e}{\bar{\varepsilon_1}^2} \tag{19}$$

5.2 Biaxial Strain and Elastic Constant C_{12}

In the case of a **biaxial strain**, both ε_{11} and ε_{22} are nonzero. The strain tensor and its Voigt notation become:

$$\varepsilon_{ij} = \begin{bmatrix} \bar{\varepsilon}_1 & 0 & 0 \\ 0 & \bar{\varepsilon}_2 & 0 \\ 0 & 0 & 0 \end{bmatrix} \quad \Rightarrow \quad \varepsilon_v = \begin{bmatrix} \bar{\varepsilon}_1 \\ \bar{\varepsilon}_2 \\ 0 \\ 0 \\ 0 \\ 0 \end{bmatrix} \tag{20}$$

The strain energy density is given by:

$$W^e = \frac{1}{2} \varepsilon_v^T \mathbf{C} \varepsilon_v \tag{21}$$

Expanding this:

$$W^e = \frac{1}{2} \begin{bmatrix} \bar{\varepsilon}_1 & \bar{\varepsilon}_2 \end{bmatrix} \begin{bmatrix} C_{11} & C_{12} \\ C_{21} & C_{22} \end{bmatrix} \begin{bmatrix} \bar{\varepsilon}_1 \\ \bar{\varepsilon}_2 \end{bmatrix} = \frac{1}{2} \left[C_{11} \bar{\varepsilon}_1^2 + 2 C_{12} \bar{\varepsilon}_1 \bar{\varepsilon}_2 + C_{22} \bar{\varepsilon}_2^2 \right] \tag{22}$$

Assuming $\bar{\varepsilon}_1 = \bar{\varepsilon}_2 = \bar{\varepsilon}$, this simplifies to:

$$W^e = \bar{\varepsilon}^2 (C_{11} + C_{12}) \tag{23}$$

Thus, if W^e is known and C_{11} is computed separately from a uniaxial test, we can solve for C_{12} as:

$$C_{12} = \frac{W^e}{\bar{\varepsilon}^2} - C_{11} \tag{24}$$

6 Shear Strain Energy and Elastic Constant C_{44}

6.1 Shear Strain State and Energy Expression

For shear deformation in the yz-plane, the relevant tensor components in index notation are:

$$W^e = \frac{1}{2} C_{44} \varepsilon_4^2 \tag{25}$$

6.2 Shear Strain Tensor Representation

The strain tensor under pure shear in the yz-plane is:

$$\varepsilon_{ij} = \begin{bmatrix} 0 & 0 & 0 \\ 0 & 0 & \bar{\varepsilon} \\ 0 & \bar{\varepsilon} & 0 \end{bmatrix} \quad \Rightarrow \quad \varepsilon_v = \begin{bmatrix} 0 \\ 0 \\ 0 \\ 2\bar{\varepsilon} \\ 0 \\ 0 \end{bmatrix} \tag{26}$$

7 Computation of Elastic Constants

The elastic stiffness constants of FCC copper were determined using energy-strain relationships. The calculations involved fitting a cubic polynomial to the potential energy variations with strain and computing the second derivative to obtain the relevant elastic moduli.

7.1 Computation of Elastic Constant C_{11}

To determine the elastic constant C_{11}, the FCC copper crystal was subjected to **uniaxial strain** along the x-axis. The variation in potential energy with strain was fitted to a cubic polynomial, as shown in Figure 7.

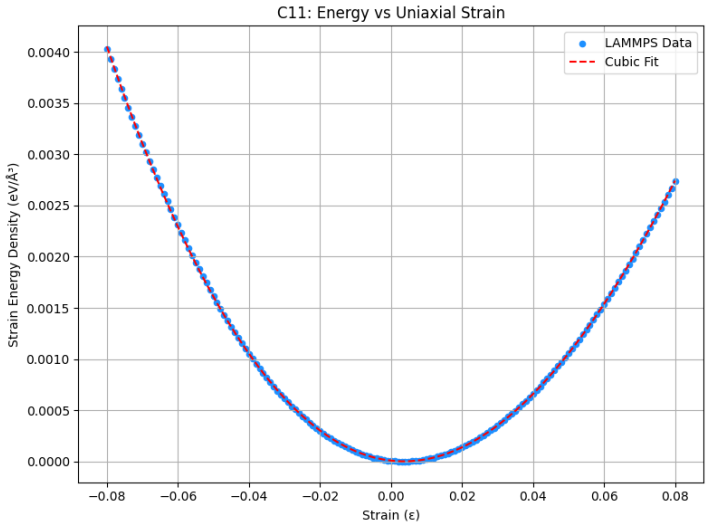

Figure 7: Curve fitting for computing C_{11}

The strain energy density function W^e as a function of strain $\bar{\varepsilon}$ is expressed as:

$$W^e = p_0 + p_1\bar{\varepsilon} + p_2\bar{\varepsilon}^2 + p_3\bar{\varepsilon}^3 \tag{27}$$

With the fitted coefficients:

$$W^e = 9 \times 10^{-6} - 0.003841\bar{\varepsilon} + 0.529298\bar{\varepsilon}^2 - 0.678996\bar{\varepsilon}^3 \tag{28}$$

The elastic constant C_{11} is obtained from the second derivative of W^e at zero strain:

$$C_{11} = \left.\frac{\partial^2 W^e}{\partial \bar{\varepsilon}^2}\right|_{\bar{\varepsilon}=0} = 2p_2 = 2 \times 0.529298 = 1.0586\,\text{eV/Å}^3 \tag{29}$$

Converting to GPa using $1\,\text{eV/Å}^3 = 160.21766208\,\text{GPa}$:

$$C_{11} = 1.0586 \times 160.2177 = 169.61\,\text{GPa} \tag{30}$$

This value agrees well with literature data for copper at room temperature.

7.2 Computation of Elastic Constant C_{12}

To determine the elastic constant C_{12}, the FCC crystal was subjected to **biaxial strain** in the x- and y-directions. The relationship between strain and potential energy is depicted in Figure 8.

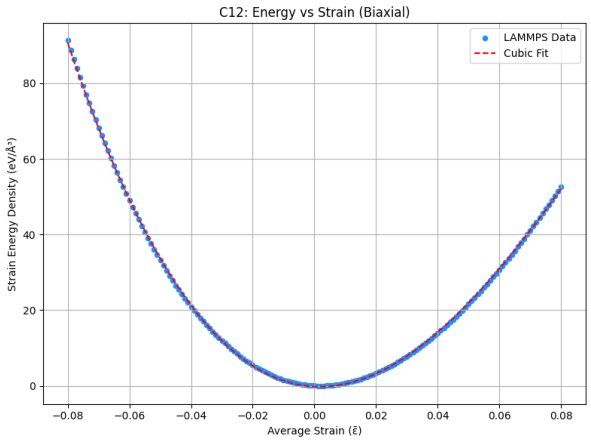

Figure 8: Curve fitting for computing C_{12}

The polynomial fit for potential energy is given by:

$$W^e = p_0 + p_1\bar{\varepsilon} + p_2\bar{\varepsilon}^2 + p_3\bar{\varepsilon}^3 \tag{31}$$

From curve fitting, the coefficients obtained were:

$$W^e = -0.2133 - 38.7353\bar{\varepsilon} + 11191.0619\bar{\varepsilon}^2 - 31643.6693\bar{\varepsilon}^3 \tag{32}$$

The elastic constant C_{12} is given by:

$$C_{12} = \frac{1}{V}\left.\frac{\partial^2 W^e}{\partial\varepsilon_1\partial\varepsilon_2}\right|_{\bar{\varepsilon}=0} \tag{33}$$

Evaluating the second derivative at zero strain:

$$\frac{\partial^2 W^e}{\partial\varepsilon_1\partial\varepsilon_2} = 2 \times 11191.0619 = 22382.1238 \text{ eV} \tag{34}$$

With simulation volume:

$$V = 5880.74 \text{ Å}^3 = 5.88074 \times 10^{-28} \text{ m}^3 \tag{35}$$

Thus, the elastic constant is:

$$C_{12} = 135.29\,\text{GPa} \tag{36}$$

7.3 Computation of Elastic Constant C_{44}

The elastic constant C_{44} was determined by applying **shear strain** in the FCC lattice and fitting the potential energy curve, as shown in Figure 9.

The cubic polynomial fit for energy-strain relationship:

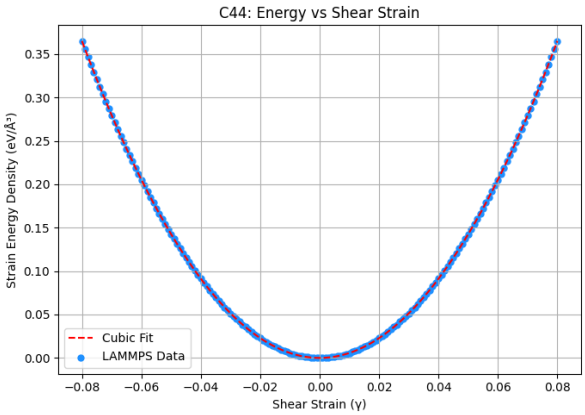

Figure 9: Curve fitting for computing C_{44}

$$W^e = 3.7158 \times 10^{-7} + 0.0002502\,\bar{\varepsilon} + 56.3455\,\bar{\varepsilon}^2 - 0.6661\,\bar{\varepsilon}^3$$

From this, the second derivative is:

$$\frac{\partial^2 W^e}{\partial \bar{\varepsilon}_4 \partial \bar{\varepsilon}_4} = 2p_2 + 6p_3\bar{\varepsilon}$$

Evaluating at zero strain ($\bar{\varepsilon} = 0$):

$$\frac{\partial^2 W^e}{\partial \bar{\varepsilon}_4 \partial \bar{\varepsilon}_4} = 2 \times 56.3455 = 112.691 \text{ eV}$$

Given the simulation volume:

$$V_0 = (a_0 \times 5)^3 = (3.61\,\text{Å} \times 5)^3 = 5880.74\,\text{Å}^3$$

Solving for C_{44}:

$$C_{44} = 0.9328 \times 10^{11}\,\text{N/m}^2$$

Converting to GPa:

$$C_{44} = 0.9328 \times 10^{11}\,\text{N/m}^2 = 0.9328\,\text{GPa}$$

7.4 Comparison of Computed Elastic Constants

A comparison of the computed elastic constants with literature values is provided in Table 5.

Elastic Constant	Literature Value	Computed Value	Error (%)
C_{11}	1.7620	1.6961	3.74%
C_{12}	1.2494	1.3550	8.29%
C_{44}	0.8177	0.9328	14.1%

Table 5: Comparison of computed elastic constants with literature values

8 Quadratic Fit of Strain Energy Density

In this task, we assumed a quadratic dependence of the potential energy density with respect to strain:

$$E(\varepsilon) = a\varepsilon^2 + b\varepsilon + c$$

This assumption is valid in the elastic regime, as described by Hooke's Law, where the potential energy varies approximately quadratically with strain near equilibrium.

To test this assumption, we performed atomistic simulations over a strain range from $\varepsilon = -0.08$ to $\varepsilon = +0.08$, and normalized the resulting potential energy with respect to the minimum energy value. The corresponding energy-strain response is plotted below.

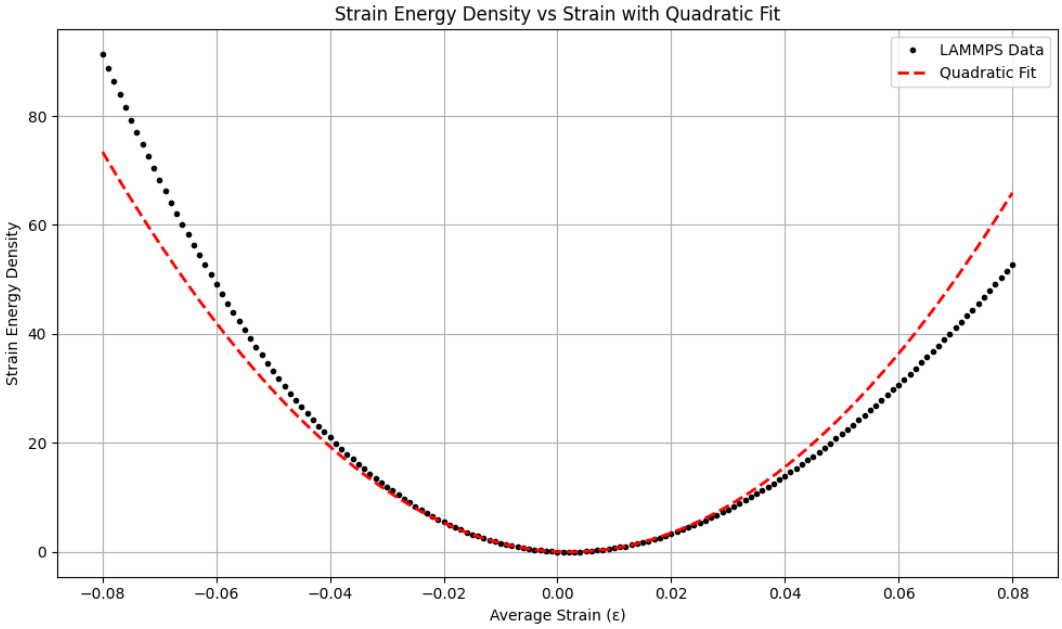

Figure 10: Strain energy Density vs. strain with a quadratic fit

8.1 Zoomed-In View and Validity of Quadratic Assumption

To better observe the behavior around the relaxed state, a zoomed-in view of the same fit is shown in Figure 11. A second-order polynomial was fitted to the energy-strain data in the small-strain range. In this range, the simulation data follows the quadratic curve very closely, validating the assumption of linear elasticity.

8.2 Deviation from Quadratic Behavior

As strain increases beyond approximately $\varepsilon = \pm 0.02$, deviations between the LAMMPS data and the fitted quadratic curve become more apparent. Specifically:

- Between $\varepsilon = \pm 0.02$ and ± 0.03, the energy rises slightly faster than the quadratic prediction.
- Beyond $\varepsilon = \pm 0.03$, the deviation becomes significant, with the actual data increasing more steeply, indicating nonlinear elastic or even anharmonic effects.

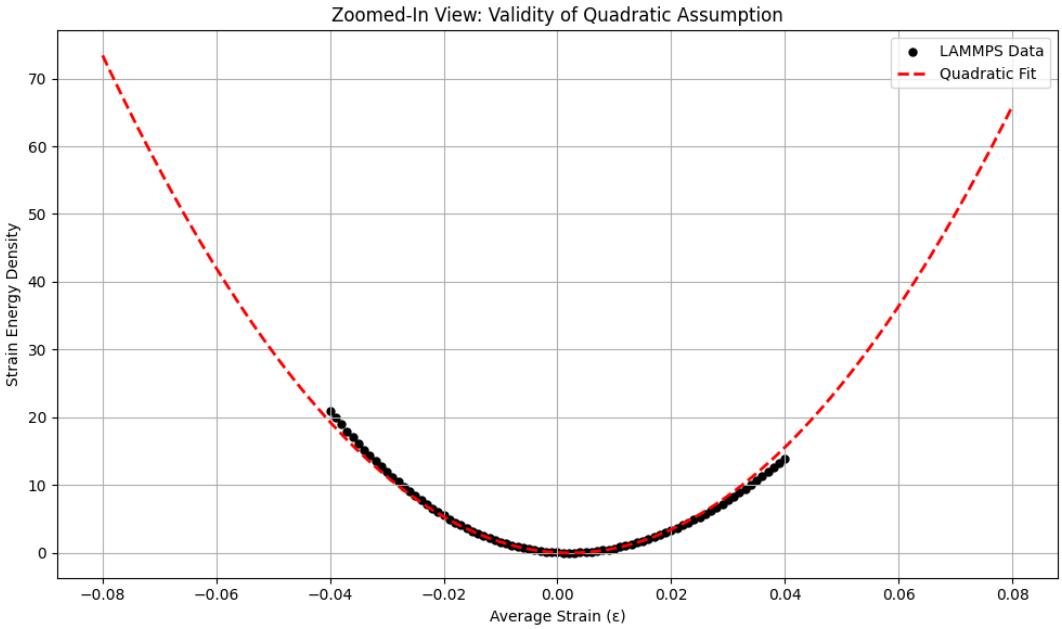

Figure 11: Zoomed-in view of strain energy curve highlighting the range of validity of the quadratic fit

Conclusion: The quadratic approximation is valid within the range $\varepsilon \in [-0.02, +0.02]$. Beyond this range, higher-order terms are necessary to capture the nonlinear response.

9 Conclusion

This study examined the structural and elastic properties of FCC copper through atomistic simulations. Key findings include:

- The equilibrium lattice constants and cohesive energies obtained from molecular dynamics simulations closely align with literature values, confirming the accuracy of the chosen potential models.
- The elastic constants C_{11}, C_{12}, and C_{44} were computed using energy-strain relationships, with deviations from reference values attributed to the choice of interatomic potentials and simulation parameters.
- The quadratic assumption in energy-strain behavior holds well for small strains up to approximately $\varepsilon = \pm 0.02$, beyond which nonlinear effects become significant and a higher-order model is required.

Overall, the study validates the effectiveness of computational modeling in predicting material behavior, while highlighting the need for higher-order corrections at large deformations.

Appendix A: Strain and Energy Data for Elastic Constants

A.1 C_{11}

Strain Values:

-0.080000, -0.079000, -0.078000, -0.077000, -0.076000, -0.075000, -0.074000, -0.073000, -0.072000,
-0.071000, -0.070000, -0.069000, -0.068000, -0.067000, -0.066000, -0.065000, -0.064000, -0.063000,
-0.062000, -0.061000, -0.060000, -0.059000, -0.058000, -0.057000, -0.056000, -0.055000, -0.054000,
-0.053000, -0.052000, -0.051000, -0.050000, -0.049000, -0.048000, -0.047000, -0.046000, -0.045000,
-0.044000, -0.043000, -0.042000, -0.041000, -0.040000, -0.039000, -0.038000, -0.037000, -0.036000,
...
0.080000

Potential Energy (eV):

-1746.2956, -1746.8788, -1747.4532, -1748.0186, -1748.5755, -1749.1240, -1749.6640, -1750.1957, -1750.7189, -1751.2338,
-1751.7405, -1752.2392, -1752.7300, -1753.2121, -1753.6848, -1754.1470, -1754.6002, -1755.0487, -1755.4964, -1755.9544,
-1756.4068, -1756.8511, -1757.2874, -1757.7157, -1758.1361, -1758.5486, -1758.9532, -1759.3499, -1759.7388, -1760.1199,
-1760.4933, -1760.8589, -1761.2169, -1761.5672, -1761.9099, -1762.2449, -1762.5725, -1762.8924, -1763.2049, -1763.5099,
-1763.8075, -1764.0977, -1764.3805, -1764.6559, -1764.9240, -1765.1849, -1765.4385, -1765.6848, -1765.9240, -1766.1560,
-1766.3809, -1766.5987, -1766.8094, -1767.0130, -1767.2097, -1767.3993, -1767.5820, -1767.7578, -1767.9267, -1768.0887,
-1768.2439, -1768.3923, -1768.5339, -1768.6687, -1768.7968, -1768.9183, -1769.0330, -1769.1412, -1769.2427, -1769.3376,
-1769.4260, -1769.5079, -1769.5833, -1769.6522, -1769.7146, -1769.7707, -1769.8204, -1769.8637, -1769.9007, -1769.9314,
-1769.9558, -1769.9740, -1769.9860, -1769.9918, -1769.9914, -1769.9849, -1769.9722, -1769.9535, -1769.9288, -1769.8980,
-1769.8612, -1769.8184, -1769.7697, -1769.7151, -1769.6545, -1769.5881, -1769.5159, -1769.4378, -1769.3540, -1769.2644,
-1769.1690, -1769.0680, -1768.9613, -1768.8489, -1768.7308, -1768.6072, -1768.4780, -1768.3432, -1768.2029, -1768.0571,
-1767.9058, -1767.7491, -1767.5869, -1767.4193, -1767.2464, -1767.0681, -1766.8844, -1766.6955, -1766.5013, -1766.3018,
-1766.0971, -1765.8872, -1765.6722, -1765.4519, -1765.2266, -1764.9961, -1764.7606, -1764.5200, -1764.2744, -1764.0237,
-1763.7681, -1763.5075, -1763.2420, -1762.9716, -1762.6963, -1762.4161, -1762.1311, -1761.8413, -1761.5467, -1761.2473,
-1760.9432, -1760.6344, -1760.3209, -1760.0027, -1759.6798, -1759.3523, -1759.0202, -1758.6836, -1758.3424, -1757.9966,
-1757.6464, -1757.2916, -1756.9324, -1756.5688, -1756.2007, -1755.8283, -1755.4515, -1755.0703, -1754.6848, -1754.2950,
-1753.9010

A.2 C_{12}

Strain Values:

-0.080000, -0.079000, -0.078000, -0.077000, -0.076000, -0.075000, -0.074000, -0.073000, -0.072000,
-0.071000, -0.070000, -0.069000, -0.068000, -0.067000, -0.066000, -0.065000, -0.064000, -0.063000,
...
0.080000

Potential Energy (eV):

-1678.6897, -1681.1776, -1683.6237, -1686.0285, -1688.3921, -1690.7151, -1692.9976, -1695.2400,
...
-1717.3128

A.3 C_{44}: Shear Strain

Strain Values:

-0.080000, -0.079000, -0.078000, -0.077000, -0.076000, -0.075000, -0.074000, -0.073000, -0.072000,
...
0.080000

Potential Energy (eV):

-1769.5908, -1769.5999, -1769.6089, -1769.6177, -1769.6264, -1769.6351, -1769.6436, -1769.6519,
...
-1769.5908

—

References

[1] N. J. Simon, E. S. Drexler, and R. P. Reed, *Properties of Copper and Copper Alloys at Cryogenic Temperatures*, NIST Monograph 177, National Institute of Standards and Technology, 1992.